Hydrophilization of Magnetic Nanoparticles with Modified Alternating Copolymers. Part 1: The Influence of the Grafting

Lyudmila M. Bronstein,*,† Eleonora V. Shtykova,‡ Andrey Malyutin,† Jason C. Dyke,† Emily Gunn,† Xinfeng Gao,† Barry Stein,§ Peter V. Konarev,† Bogdan Dragnea,† and Dmitri I. Svergun*,†

Department of Chemistry, Indiana University, 800 E. Kirkwood Avenue, Bloomington, Indiana 47405, United States, Institute of Crystallography, Russian Academy of Sciences, Leninsky pr. 59, 117333 Moscow, Russia, Department of Biology, Indiana University, 1001 East Third Street, Bloomington, Indiana 47405, United States, and EMBL, Hamburg Outstation, Notkestrasse 85, D-22603 Hamburg, Germany

Received: August 3, 2010; Revised Manuscript Received: October 11, 2010

Iron oxide nanoparticles (NPs) with a diameter of 21.6 nm were coated with poly(maleic acid-*alt*-1-octadecene) (PMAcOD) modified with grafted 5000 Da poly(ethyelene glycol) (PEG) or short ethylene glycol (EG) tails. The coating procedure utilizes hydrophobic interactions of octadecene and oleic acid tails, while the hydrolysis of maleic anhydride moieties as well as the presence of hydrophilic PEG (EG) tails allows the NP hydrophilicity. The success of the NP coating was found to be independent of the degree of grafting, which was varied between 20 and 80% of the −MacOD− units, but depended on the length of the grafted tail. The NP coating and hydrophilization did not occur when the modified copolymer contained 750 Da PEG tails independent of the grafting degree. To explain this phenomenon, the micellization of the modified PMAcOD copolymers in water was analyzed by small-angle X-ray scattering. The PMAcOD molecules with the grafted 750 Da PEG tails form compact noninteracting disklike micelles, whose stability apparently allows for no interactions with the NP hydrophobic shells. The PMAcOD containing the 5000 Da PEG and EG tails form much larger structures capable of an efficient coating of the NPs. The coated NPs were characterized using transmission electron microscopy, dynamic light scattering, ζ-potential measurements, and thermal gravimetry analysis. The latter method demonstrated that the presence of long PEG tails in modified PMAcOD allows the attachment of fewer macromolecules (by a factor of ∼20) compared with the case of nonmodified or EG-modified PMAcOD, emphasizing the importance of PEG tails in NP hydrophilization. The NPs coated with PMAcOD modified with 60% (toward all −MAcOD− units) of the 5000 PEG tails bear a significant negative charge and display good stability in buffers. Such NPs can be useful as magnetic cores for virus-like particle formation.

1. Introduction

Magnetic nanoparticles (NPs) with hydrophilic shells have received considerable attention because of their promising bioapplications, such as biosensors,[1,2] contrast enhancement agents for magnetic resonance imaging,[3−7] bioprobes,[8−11] etc. In the majority of these applications, it is important to use NPs with a narrow particle size distribution because magnetic properties are size-dependent.[12−15] Iron oxide NPs are commonly recommended for bioapplications because they are easily metabolized or degraded in vivo.[16,17] Monodisperse iron oxide NPs can be prepared by thermal decomposition of iron acetylacetonates[18−20] or carboxylates[20−24] in high-boiling solvents in the presence of such surfactants as oleic, palmitic, and other fatty acids and/or oleylamine. In all these methods, the NPs are coated with fatty acids or amines and soluble only in a few organic solvents. On the other hand, hydrophilicity and biocompatibility are required for all biomedical applications.

There are several methods to impart water solubility (hydrophilicity) and biocompatibility. They are a place (ligand)-exchange reaction,[25−29] placement of polymer chains on a nanoparticle surface,[30,31] NP growth in the presence of polymeric surfactants,[32] or coating of NPs with amphiphilic molecules due to formation of hydrophobic double layers.[33−35] The last method was shown to be particularly facile for the NP hydrophilization.[33−35] The encapsulation of monodisperse iron oxide NPs by PEGylated phospholipids was described in our preceding papers.[36,37] This coating yields stable hydrophilic magnetic NPs of different sizes and shapes that are also well compatible with various buffers and physiological solutions. The only downside of PEGylated phopsholipids as coating agents to yield hydrophilic NPs is the high cost that hampers their application.

Alternating amphiphilic copolymers showed promise for NP functionalization.[38,39] The encapsulation of hydrophobic NPs with short (7300 Da) poly(maleic anhydride-*alt*-1-tetradecene) was described in ref 38. To stabilize the polymer coating, the authors used cross-linking of the alternating copolymer anhydride groups with bis(6-aminohexyl)amine. In a preceding paper, we reported a successful encapsulation of even large magnetic NPs (16−21 nm in diameter) (the larger the particles from the same material, the stronger the magnetic attraction) using poly(maleic anhydride-*alt*-1-octadecene) (PMAOD), with a molecular weight of 30 000−50 000 Da. The longer copolymer

* To whom correspondence should be addressed. E-mail: lybronst@indiana.edu (L.M.B.), svergun@embl-hamburg.de (D.I.S.). Tel: +1-812-855-3727 (L.M.B.),+49 40 89902 125 (D.I.S.). Fax: +1-812-855-8300 (L.M.B.), +49 40 89902 149) (D.I.S.).
† Department of Chemistry, Indiana University.
‡ Russian Academy of Sciences.
§ Department of Biology, Indiana University.
† EMBL.

10.1021/jp107283w

compared with that reported in ref 38 provides a stable NP shell without additional cross-linking accompanying with the loss of carboxyl groups (decreased negative charge), whereas the longer hydrophobic tail (C_{16} vs C_{12} in the previously studied copolymer[38]) allows the more stable hydrophobic double layer. Interestingly, in a recent paper by Di Corato et al.,[40] the same PMAOD was used as well for NP coating; however, the authors again employed cross-linking with an amine for coating stabilization, which we proved to be unnecessary. In water, PMAOD is easily hydrolyzed, yielding poly(maleic acid-*alt*-1-octadecene), PMAcOD, where maleic acid units are highly hydrophilic and negatively charged.[41]

In our preceding paper we reported PMAcOD self-assembling in water and the structure of NPs coated with PMAcOD.[41] It was demonstrated that NPs with a PMAcOD coating are stable for many months without changes of their characteristics or aggregation. However, these NPs were only stable in water, whereas the addition of salt immediately resulted in NP aggregation because the NP stabilization here is purely electrostatic and it is screened when a salt is added. To impart stability in buffers and physiological solutions to NPs, steric stabilization is required. In the present paper, we report the coating of iron oxide NPs with a diameter of 21.6 nm with altered PMAODs containing grafted poly(ethylene glycol) (PEG) or short ethylene glycol (EG) brushes. This type of alteration was described in ref 39 using 6000 Da PEG with an amino or hydroxyl terminal group or a number of PEGs with different molecular weights in the following paper of the same authors.[42] However, although, in ref 42, PEG−NH_2 with molecular weights of 6000, 9900, and 19 300 Da and PEG−OH with molecular weights of 550, 750, and 2000 Da were mentioned for PMAOD alteration, it was not specified anywhere in the paper that these copolymers were equally successful in NP coating.

In the present work, we studied the dependence of the coating on the density of the grafted brush and on the PEG chain length. Discovery of the surprising phenomenon that PMAOD−PEG with a 750 Da PEG tail does not coat NPs, whereas PMAOD−PEG with 5000 Da PEG and PMAOD−EG do, prompted a synchrotron small-angle X-ray scattering (SAXS) study of the micellization of the modified PMAcOD in water. Using the advanced SAXS data analysis methods, it became, for the first time, possible to establish a link between the properties of micellar solutions and the ability of an alternating copolymer to efficiently coat the NPs. The NPs coated with modified PMAcODs were characterized using transmission electron microscopy (TEM), dynamic light scattering (DLS), ζ-potential measurements, and thermal gravimetric analysis (TGA).

2. Experimental Section

2.1. Materials. Hexanes (85%), ethanol (95%), and acetone (99.78%) were purchased from EMD and used as received. Chloroform (Mallinckrodt, 100%), $FeCl_3 \cdot 6H_2O$ (98%, Aldrich), docosane (99%, Aldrich), oleic acid (OA, 90%, Aldrich), oleic acid sodium salt (97%, TCI), and TBE buffer (1.3 M Tris, 450 mM boric acid, 25 mM EDTA·Na_2 in H_2O, Fluka) were used without purification. PMAOD (30 000−50 000 Da, Aldrich) was used as received. *O*-(2-aminoethyl)-*o*′-methyl polyethylene glycols with MW = 5000 and MW = 750 (PEG−NH_2) and (±)-3-amino-1,2-propanediol (98.0%) (EG) were purchased from Fluka and used as received. Water was purified with a Milli-Q (Millipore) water purification system (18 μS).

2.2. Synthetic Procedures. ***2.2.1. Synthesis of Iron Oxide Nanoparticles.*** For the detailed procedure, see our preceding paper.[43] The synthesis of iron oleate was carried out according to the published procedure.[22] Iron oleate was then purified and dried for 24 h at room temperature and for 20 h at 70 °C in the vacuum oven. Spherical iron oxide nanoparticles 21.6 nm in diameter were prepared through thermal decomposition of iron oleate in the presence of oleic acid in docosane as a solvent.[43] The round-bottom three-neck flask was charged with 1.91 g of iron oleate, 7.02 g of docosane, and 0.93 mL of oleic acid. The flask was evacuated three times and filled with argon afterward. The flask was then heated to 70 °C to melt docosane, and then a vigorous stirring was set. The reaction mixture was heated to ∼370 °C with a heating rate of 3.3 °C/min and was allowed to stir at this temperature for 5 min. The reaction mixture was then allowed to cool to 60 °C and was placed in a vial while it is a liquid. At room temperature, the reaction solution solidifies, allowing for the long-term storage of NPs. When needed, the waxy NP solid is melted with a heat gun and precipitated with a mixture of acetone and hexane (5:1), followed by two consecutive washings with mixtures of acetone and hexane with volume ratios of 3:1 and 1:1. The NP solution is centrifuged after each wash to remove side products. The NPs are easily resuspended in chloroform after the final wash. The yield is 84%. The TEM image of these NPs is shown in the Supporting Information (Figure S1).

2.2.2. Synthesis of PMAOD−PEG(EG) Copolymers. To encapsulate the iron oxide NPs in PMAOD−PEG(EG), first, modified PEG polymers were synthesized. Notations "P", "S", and "G" are reserved for PMAOD−PEG(5000), PMAOD−PEG(750), and PMAOD−EG, respectively. Mole ratios of 1:20 (P1, S1, G1), 1:30 (P2, S2, G2), 1:60 (P3, S3, G3), and 1:80 (P4) of PMAOD to PEG or EG were used. The stock solutions of these samples were prepared in chloroform. The PMAOD stock solution (10.0 mg/mL) was also prepared in chloroform. For a typical modified stock solution with a mole ratio of PMAOD/PEG−NH_2 = 20:1 (P1; see Table S1, the Supporting Information, for notations), 37.5 mg of 5000 Da PEG−NH_2 was dissolved in 1 mL of $CHCl_3$ and sonicated for 10 min. Upon completion, 1.5 mL of the PMAOD stock was added and the solution was allowed to stir overnight. Table S1 (the Supporting Information) summarizes the amounts of reagents for the modified PMAOD synthesis and the yields of the copolymers.

2.2.3. Encapsulation of Iron Oxide Nanoparticles with PMAOD−PEG(EG) Copolymers. For nanoparticle encapsulation, a 1:1 mass ratio between iron oxide NPs and PMAOD was maintained, except for the EG stock solutions, where the 1:1.5 ratio was employed. In a typical experiment, 1 mg of NPs was combined with 0.17 mL of the P1 stock solution. The mixture was allowed to stir for 1 h. Chloroform was then evaporated under vacuum, and 2 mL of 20% TBE buffer was added. After sonicating for 10 min, the solution was heated at 60 °C for an additional 10 min. The mixture was allowed to stir overnight. The following day, the polymer excess was removed by ultracentrifugation (1 h, 90 000 rpm/440 kg). The supernatant was discarded and the NP pellet resuspended in water. Aggregates were removed by low-speed centrifugation. The isolated yield was not taken because of the small scale of the reaction.

2.2.4. Hydrolysis of Modified PMAOD. The solutions of modified PMAOD (2 mL each; P3, 7.84 mg/mL; S3, 6.4 mg/mL; and G3, 7.4 mg/mL) in $CHCl_3$ were evaporated in a vacuum oven. To the dried samples, 2 mL of 20% TBE buffer was added, and the solutions were stirred for 24 h.

2.3. Characterization. Dynamic light scattering (DLS) and ζ-potential measurements were performed using a Malvern Zetasizer Nano ZS. For the DLS measurements, typically, the diluted sample in water (concentration was in the range of 0.05−0.15 mg/mL) underwent sonication for about 10−20 min and filtration with a 0.2 μm syringe filter before the measurement. The measurement duration was set to be determined automatically, and data were averaged from at least three runs. Intensity and volume distributions of the particle sizes were recorded.

The ζ-potential was measured at pH 7.4. Data were processed using the absorption of bulk iron oxide, the indices of refraction of iron oxide and solvent, and the viscosity of the pure water. The Smoluchowski approximation was used to convert the electrophoretic mobility to a ζ-potential.

Electron-transparent specimens for TEM were prepared by placing a drop of a dilute solution onto a carbon-coated Cu grid. Images were acquired at an accelerating voltage of 80 kV on a JEOL JEM1010 transmission electron microscope. Images were analyzed with the ImageJ software package to estimate NP diameters. Normally, 150−300 NPs were used for analysis.

Thermal gravimetric analysis (TGA) was performed on a TGAQ5000 IR manufactured by TA Instruments. The TGA samples were prepared in the following way. An aqueous solution of the NP sample coated with a copolymer was evaporated, and the NPs were resuspended in the minimum amount of chloroform. The solution was completely transferred into a 100 μL platinum pan, by filling the pan and allowing chloroform to evaporate. The experiments were carried out upon heating to 700 °C with a rate of 10.0 °C/min.

The composition of modified PMAOD was studied by NMR. All NMR samples were dissolved in $CDCl_3$, and all spectra were recorded on a Varian UNITY INOVA 500 MHz spectrometer at 25 °C, unless stated otherwise. ^{1}H, ^{13}C, and ^{13}C DEPT (distortionless enhancement by polarization transfer); ^{1}H DQF-COSY (double-quantum-filtered correlation spectroscopy); and ^{13}C−^{1}H HSQC (heteronuclear single quantum correlation) experiments were performed. The ^{1}H and ^{13}C spectral assignments were made based on the results of these experiments and the spectral simulation results using ACD HNMR and CNMR Predictor 9.0 software. Spin−lattice relaxation times (T_1) were measured for these samples using an inversion recovery method. The T_1 values determined for each ^{13}C peak of these samples were in the range of 0.8−5.5 s. These values were used to optimize NMR parameters for quantitative ^{13}C measurements. The inverse gated decoupling ^{13}C{^{1}H} NMR experiments, with an acquisition time of 0.8 s, pulse delay of 7 s, and pulse flip angle of 30°, were performed for the quantitative measurements.

The synchrotron radiation X-ray scattering measurements were done in the European Molecular Biology Laboratory (EMBL) on the storage ring DORIS III of the Deutsches Elektronen Synchrotron (DESY, Hamburg) on the X33 camera with a MAR Image plate detector.[44] The scattering was recorded in the range of the momentum transfer, $0.07 < s < 5.0$ nm^{-1}, where $s = (4\pi \sin \theta)/\lambda$, 2θ is the scattering angle, and $\lambda = 0.15$ nm is the X-ray wavelength. All measurements were carried out in a vacuum cuvette to diminish the parasitic scattering, and the samples were exposed in four 30 s frames to monitor for possible radiation damage. Three sets of modified PMAcOD samples with four different concentrations in solution were studied by SAXS: (1) P3 with the solution concentrations of 1, 2, 3, and 7.84 mg/mL; (2) S3 with the solution concentrations of 1, 2, 3, and 6.4 mg/mL; and (3) G3 with the solution concentrations of 1, 2, 3, and 7.4 mg/mL. The scattering profiles were corrected for the background scattering from distilled water and processed using standard procedures.[45]

SCHEME 1: Repeating Unit of the Modified PMAOD[a]

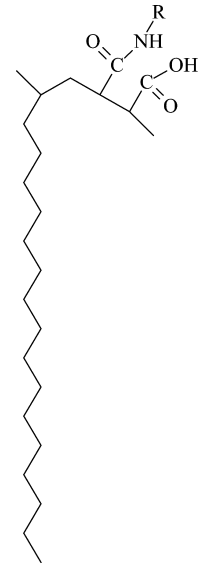

[a] R is either PEG−NH_2 (MW = 5000 or 750 Da) or EG.

The distance distribution functions $p(r)$ of the self-assembled nanoparticles of the modified PMAcODs were calculated using an indirect transform program GNOM.[46] Low-resolution shapes and the internal structure of the micelles of the grafted copolymer were reconstructed ab initio from the scattering patterns using the program DAMMIN.[47] The SAXS patterns from the modeled structures of the modified PMAcODs in solution were calculated using the program CRYSOL[48] and compared with the experimental scattering curves.

3. Results and Discussion

3.1. Synthesis and Characterization of Modified PMAOD. PMAOD contains an anhydride moiety in each polymer unit; thus, this moiety can easily interact with an amino group of various compounds with the formation of amide and carboxyl groups (Scheme 1). We varied the amount of grafted hydrophilic tails in the range of 20−80% of all anhydride groups[39,42] to determine its influence on the NP coating. To establish the influence of the concentration of the reagents on the degree of grafting, we used two very different concentrations: 1.67×10^{-5} and 6.3×10^{-4} M.

NMR was employed to quantitatively evaluate the proportion of grafting at different conditions. The NMR data (see the Supporting Information) revealed that, at the concentration of 6.3×10^{-4} M, the reaction goes to completion for any degree of grafting (except for S3). At the lower concentration (1.67×10^{-5} M), the attachment is complete for 20% and 30% grafting, whereas for the polymers with an intended 60% or higher degree of grafting, approximately 20−30% of the PEG−NH_2 molecules remained unreacted in the reaction solution. Unlike other copolymers, for S3, there is incomplete grafting even in concentrated solutions. The ^{13}C NMR spectrum of S3 contains residual signals of NH_2*CH_2*CH_2O at 41.7 and 73.3 ppm, indicating the presence of unreacted PEG−NH_2 (about 20%; see details in the Supporting Information).

After attaching the grafted tails, the copolymers were hydrolyzed in 20% TBE buffer to transform unreacted anhydride moieties to carboxyl groups. Because all these copolymers are amphiphilic, that is, the octadecene tail is hydrophobic, whereas

TABLE 1: Hydrodynamic Diameter (D_h) and ζ-Potential of Modified PMAcOD at pH 7.4

copolymer	D_h (nm)	ζ-potential (mV)
G3	21.2	−59.7
S3	22.7	−49.0
P3	21.6	−40.7

the carboxyl groups along the PMAcOD chain and the grafted tails are hydrophilic, we expected self-assembling of these copolymers in water into micelle-like structures. These structures were characterized by DLS and ζ-potential measurements (Table 1).

From the data presented in Table 1, the hydrodynamic diameter of the structures formed by G3, S3, and P3 does not depend on the length of the hydrophilic tail: all hydrolyzed copolymers showed approximately the same size micelles. This seems to be counterintuitive: It was believed that P3 would have the largest diameter due to the massive 5000 Da PEG tails. Such inconsistencies of DLS data could be explained if the micelles formed are not spherical. Indeed, as reported in our preceding paper,[41] PMAcOD forms disklike structures in water, so in the case of modified PMAOD, the analogous structures could be expected.

ζ-potential values were found to be more in accordance with our expectations. Because of the same amount of grafting, the amount of the remaining charges should be the same, but the charges can be differently exposed due the presence of the hydrophilic tails. Indeed, P3 showed the smallest negative ζ-potential value at pH 7.4. It is believed that the large PEG tails are shielding the charges. The effect of shielding decreases with decreasing the molecular weight of the grafted tail.

3.2. Coating of Nanoparticles with Modified PMAcOD. The coating procedure utilizes hydrophobic interactions of octadecene and oleic acid tails, while hydrolysis of maleic anhydride moieties as well as hydrophilic PEG (EG) tails allows the NP hydrophilicity. Figure 1 presents TEM images of NPs coated with G3 and P3 copolymers. The negative staining with uranyl acetate also provides a positive staining due to interaction of carboxyl groups with uranyl cations. Thus, the PMAcOD backbone containing a carboxyl group is accentuated with the stain. The thicknesses of the shells (without PEG or glycol tails, which are invisible with this staining) for NP-P3 and NP-G3 are 3.4 and 3.7 nm, respectively.

3.2.1. DLS and ζ-Potential Data. To coat NPs with modified PMAcOD, we used a procedure described in our preceding paper[41] where a solid mixture of NPs and a copolymer after evaporation of chloroform from a mixed solution was resuspended and hydrolyzed in 20% TBE buffer (see details in the

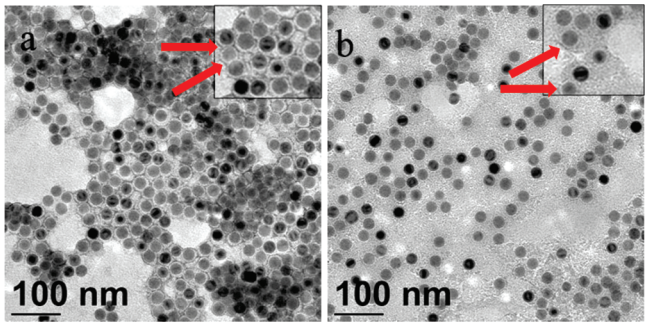

Figure 1. TEM images of NP-P3 (a) and NP-G3 (b) stained with uranyl acetate. Red arrows show the places where the positive staining can be seen despite the negative staining. Insets show higher-magnification images.

TABLE 2: Characteristics of NPs Coated with Modified PMAcOD

sample	D_h[a] (nm)	ζ-potential (mV)
NP-PMAcOD	34.0	−47.3
NP-P1	39.8	−47.0
NP-P2	43.6	−39.9
NP-P3	56.0	−30.9
NP-P4	63.0	−21.3
NP-G1	58.9	−53.2
NP-G2	70.1	−54.0
NP-G3	69.3	−33.7

[a] From DLS measurements.

Experimental Section).[41] This procedure allows a successful coating of various NPs with the P1, P2, P3, P4, G1, G2, and G3 copolymers, whereas no NPs were successfully (individually) coated with S1, S2, or S3. During the hydrolysis step, only aggregates are observed. An alternative two-phase procedure, as described elsewhere,[39] where a chloroform solution of NPs and S1, S2, or S3 was mixed with water, followed by slow removal of chloroform by rotary evaporation at room temperature, was also attempted. However, this procedure yielded a similar result: NP aggregation in aqueous solution. In section 3.3, we discuss the causes of this phenomenon.

The DLS and ζ-potential data for the NP samples coated with modified PMAcOD are shown in Table 2.

The negative charge of NPs coated with modified PMAcOD should depend on the degree of grafting: the higher the degree of grafting, the lower the charge as a fraction of carboxylic groups decreases. Indeed, this trend is observed for both the P and the G series, although for the latter, it is less pronounced. The G1 and G2 and P1 and P2 samples differ only by 10% in grafting, so the ζ-potentials values can be close within an experimental error. On the other hand, for the P series, the additional effect, that is, shielding of the charges, can take place when the grafting degree increases, thus making the difference between ζ-potentials more pronounced.

As for hydrodynamic diameters, the dependence is straightforward for the P series: the higher the degree of grafting, the larger the size. This is due to increased stretching of the PEG coils when the PEG brush density increases. For the G series, one would expect the lack of the size dependence on the grafting density as EG is very short. Nevertheless, from G1 to G2 and G3, the hydrodynamic diameter increases, which can be explained by increasing the fraction of the NP aggregates, when the negative charge decreases, thus weakening the electrostatic repulsion between NPs.

3.2.2. TGA Data. To determine the amount of modified PMAcOD molecules on the NP surface, TGA measurements were carried out. First, the amount of oleic acid molecules on the as-prepared NPs has been determined by TGA (see the Supporting Information, Figure S3) using a weight loss of 14.3% upon heating to 700 °C. An area of 1 nm^2 of the NP surface was found to contain 7.34 OA molecules.

As is discussed earlier, the coating of NPs with PMAcOD or modified PMAcOD occurs due to hydrophobic interactions of OA tails and octadecene tails;[41] thus, OA molecules are not removed during coating, if they are adsorbed on the NP surface. We have previously demonstrated, however, that, even if NPs contain excess OA, it is perfectly removed upon coating with these copolymers.[41] However, preparing the samples for TGA measurements, we made sure using FTIR that the sample contains no excessive OA (no band at 1711 cm^{-1}), so we assumed that the amount of OA is constant in all the samples

TABLE 3: Weight Losses and the Amount of Copolymer Molecules per NP for the Modified PMAcOD Coated NPs

sample	weight loss (%)	copolymer molecules per NP
PMAOD	45.5	417
P3	32.3	21
P4	34.3	19
G2	50.0	398
G3	55.4	465

and the OA weight loss can be subtracted from the weight loss of other samples for calculation of the attached copolymer molecules. The TGA weight losses and the calculated amount of copolymer molecules per each NP are presented in Table 3 (see details in the Supporting Information, also Figure S4). It should be noted that, for each data point, at least three TGA experiments have been run.

The TGA data demonstrate that the PMAOD- or G-coated NPs carry approximately 400+ copolymer molecules on each NP, whereas the amount of copolymer macromolecules on the NPs coated with P copolymers is only 19−20. For the P3 and P4 samples, this can be explained by the large amount of the long PEG tails (5000 Da) in the NP exterior creating a highly hydrophilic environment with a few copolymer molecules and preventing the attachment of more copolymer molecules to the NP surface.

3.3. Small-Angle X-ray Scattering. To understand the reasons for the different coating behavior of the S series copolymers compared with that of the copolymers of the P and G series, micellization of the modified PMAcOD samples in aqueous solutions was studied using SAXS.

The experimental scattering profiles (Figure 2a) demonstrate that the three types of micelles have different dependences on the solute concentrations. For G3 samples, we observed a strong increase in the overall size with increasing concentration; for the P3 set, the dependence was also present, but weak. For the S3 samples, the scattering patterns taken at different concentrations were superimposable within the experimental noise. All the experimental profiles display a broad peak at higher angles, characteristic for micellar systems and resembling the SAXS pattern of pure PMAcOD discussed in our previous work[41] (see the comparison in Figure 2b).

Given the concentration dependence, the distance distribution functions $p(r)$ were calculated separately for individual concentrations (Figure 3). These functions reveal bimodal profiles characteristic for bilayers; whereas the $p(r)$ for the PMAcOD copolymer displays negative values in the range of interatomic distances around 3−4 nm (Figure 3, inset), the distributions for the modified copolymers remain positive.

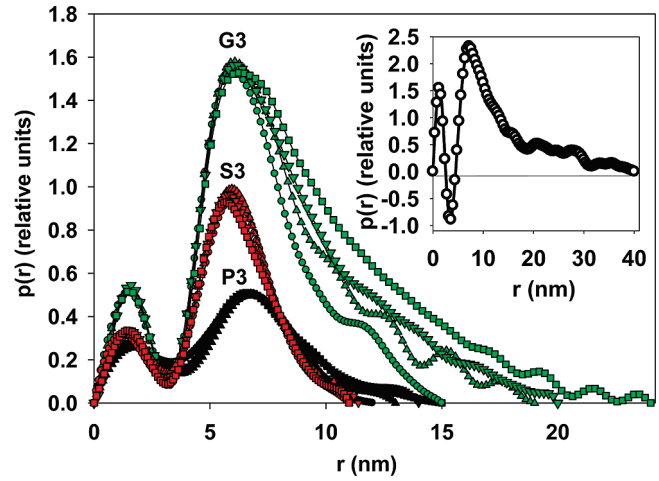

Figure 3. Distance distribution functions for the P3, S3, and G3 samples at different concentrations: P3 with the solution concentrations of 1.0 (circles), 2.0 (triangle up), 4.0 (triangle down), and 7.84 mg/mL (square); S3 with the solution concentrations of 1.0 (circles), 2.0 (triangle up), 4.0 (triangle down), and 6.4 mg/mL (square); and G3 with the solution concentrations of 1.0 (circles), 2.0 (triangle up), 4.0 (triangle down), and 7.4 mg/mL (square). Inset: the distance distribution function for the PMAcOD copolymer in solution.[41]

The negative values for the pure PMAcOD copolymer are typical for lipid bilayer structures and appear due to the well-ordered hydrophobic regions in the copolymer, which have a lower electron density than that of water and thus a negative contrast. The distances of 3−4 nm correspond to the bilayer width of the PMAcOD (1.6 nm for a single tail). Therefore, the observed changes in the $p(r)$ functions for the modified PMAcOD copolymer point to alterations in the bilayer structures, which become less ordered upon modification.

The length of the grafting tail affects the interactions between the copolymer micelles. The radii of gyration R_g and the maximum diameters D_{max} depend on the concentration for the P3 and G3 sets, but not for S3 (Figure 4).

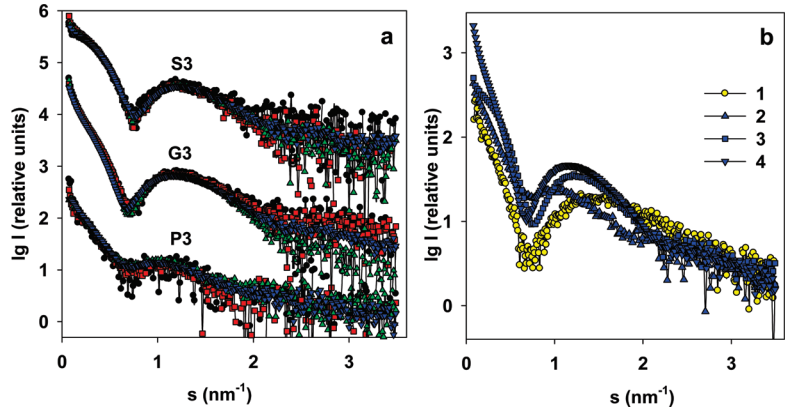

Figure 2. (a) Experimental SAXS profiles from the copolymers in solution for the samples P3, G3, and S3: P3 with the solution concentrations of 1.0 (black circles), 2.0 (red squares), 4.0 (green triangles up), and 7.84 (blue triangles down); G3 with the solution concentrations of 1.0 (black circles), 2.0 (red squares), 4.0 (green triangles up), and 7.4 mg/mL (blue triangles down); and S3 with the solution concentrations of 1.0 (black circles), 2.0 (red squares), 4.0 (green triangles up), and 6.4 mg/mL (blue triangles down). The patterns belonging to different copolymers are appropriately displaced along the logarithmic axis for better visualization. (b) A comparison of scattering profiles at the highest concentration for PMAcOD (1), P3 (2), G3 (3), and S3 (4).

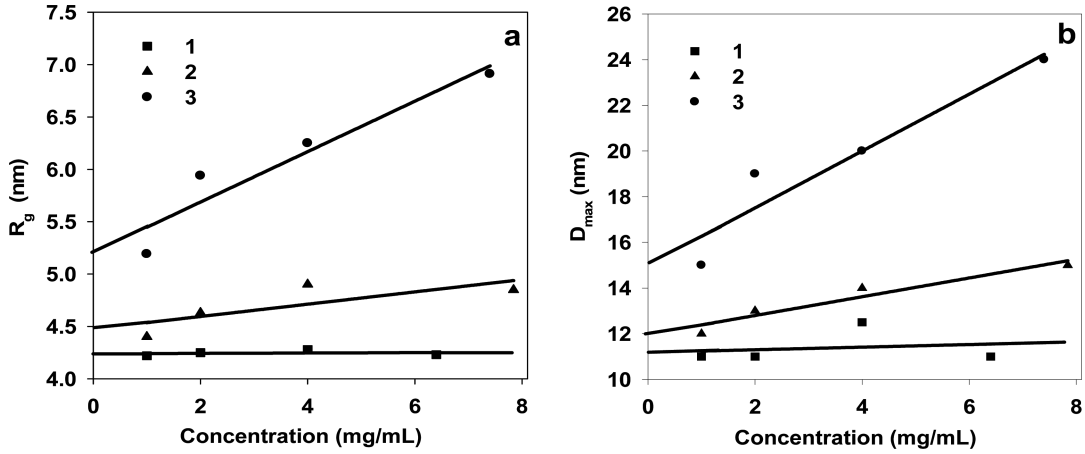

Figure 4. Dependence on the concentration (a) for radii of gyration of (1) the S3 samples ($R_{g0} = 4.24$), (2) the P3 samples ($R_{g0} = 4.47$), and (3) the G3 samples ($R_{g0} = 5.2$) and (b) for maximum diameters for (1) the S3 samples ($D_0 = 11.0$), (2) the P3 samples ($D_0 = 12.0$), and (3) the G3 samples ($D_0 = 15.0$). R_{g0} is the radius of gyration (R_g) extrapolated to zero concentration. D_0 is the maximum size (D_{max}) extrapolated to zero concentration.

As one can see from Figure 4, the micelles formed from PMAcOD modified by short glycol brushes (the G3 set) strongly interact in solution, which may facilitate interactions with NPs during coating. The regression for P3 displays a weaker dependence (less pronounced interactions), whereas the S3 set has no interactions at all. The latter micellar structures appear, therefore, as stable formations not interacting with each other, which may impair also their interactions with NPs.

To further assess the organization of the modified PMAcOD self-assemblies, models were constructed using MAcOD molecules generated in our previous work[41] with an addition of appropriate glycol molecules to the head of MAcOD.

For pure PMAcOD, disklike particles with a diameter of 40 nm and a thickness of the bilayer of 3.2 nm[41] were found to be the only type of self-assembled structures in solution. Similar to the previous work, the modified −MAcOD− units were used to construct bilayer disks, but also other geometrical structures containing bilayers. Their SAXS patterns calculated using CRYSOL[48] were compared with the experimental scattering. When disklike models were used, good fits were obtained for the S3 and G3 samples (other bilayer shapes, such as spheres or long cylinders, did not provide good fits), whereas for the P3 samples, no fit could be found for any geometrical shape. The experimental scattering curve for the P3 copolymer appears smeared compared with those of the G3 or S3 samples, reflecting possible disruptions of the bilayer structure. This loss of regularity is probably caused by the interactions between the long and heavy PEG chains. To assess the shape of the P3 sample, ab initio dummy atom modeling was employed using the program DAMMIN.[47]

The best models for the G3, S3, and P3 samples along with their fits to the experimental data are presented in Figure 5. The obtained parameters of the model disk for the G3 sample were the diameter of 18 nm and the width of the bilayer of 4.8 nm, and for the S3 sample, the diameter was found to be 10 nm, whereas the width of the bilayer was estimated to be 5.0 nm. Note that the S3 pattern could be fitted very well, whereas the calculated pattern for G3 displays deviations at small angles, whereby the experimental data indicate a larger overall size of the aggregates. However, further increase of the diameter of the G3 disk leads to systematic deviations at higher angles. It is conceivable that the G3 samples contain aggregates of the disklike micelles at the concentration used in the calculations (7.4 mg/mL).

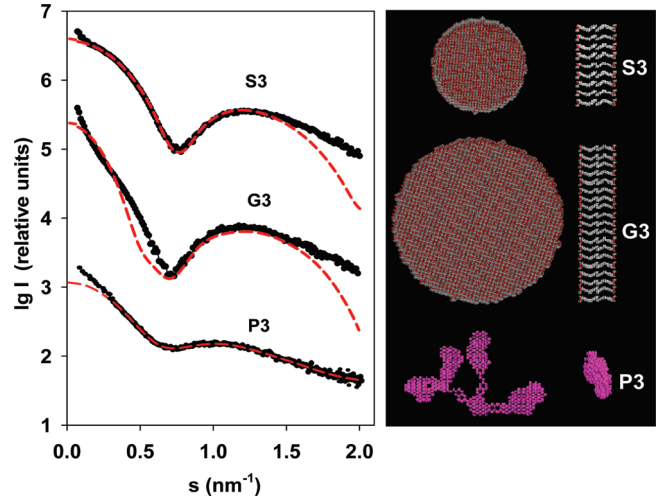

Figure 5. Modeling and the best fits: the experimental scattering curve from the modified PMAcOD copolymer in solution (black circles) and the best fits to the experimental profile of the scattering patterns computed from models (red dotted lines). Modeling was performed at maximal concentrations to reduce the influence of the experimental noise. The right panel: disklike models for the S3 and G3 samples in two orientations and a dummy atom model for the P3 specimen. Separately, a structure of the dense formations in the body of the P3 micelles is shown.

Owing to the complexity of the modified PMAcOD units for the S3 and G3 samples, we could only use hypothetical models of the monomeric units. Nevertheless, the models obtained allow us to meaningfully analyze the possibility of creating protective shells using these structures. Both the G3 and the S3 samples form ordered bilayers. However, the S3 structures are much smaller, and the micelles do not interact in solution. It appears that the S3 macromolecules form quite dense, stable structures, which are energetically favorable and do not promote interactions with external hydrophobic objects, such as NPs. The micelles of the G3 and especially of the P3 copolymers are less stable, and the NPs are able to compete with the copolymer self-assembly, leading to successful coating. The ab initio model of the P3 samples appears as an agglomerate of loosely connected subunits. The shape of these subunits restored by the program DAMMIN using a portion of the experimental scattering curve at higher angles from 2.5 up to 3.5 nm^{-1} reveals a slightly oblate body with a diameter of about 5.5 nm (Figure 5). A tentative model of the overall structure of the P3 samples

SCHEME 2: Hypothetical Model of the Structure of the P3 Copolymer in Solution

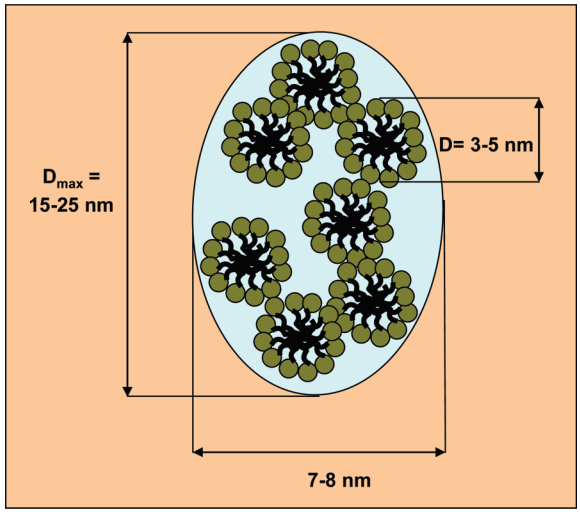

SCHEME 3: Hypothetical Model of Partial Segregation in Micellar Bilayers

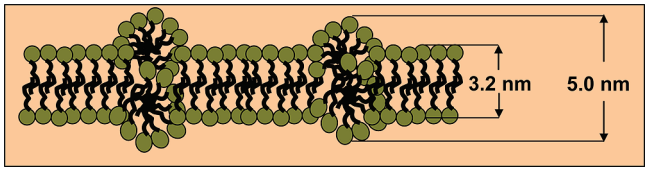

can be represented as a mesh of segregated sections of the modified copolymer, which are small micelles of the PMAcOD chains with diameters of about 5.0−5.5 nm covered by layers of the PEG molecules, most probably in a bent conformation (Scheme 2). The geometrical parameters of the model indicated in Scheme 2 correspond to the dimensions calculated from the $p(r)$ function for this sample (Figure 2).

It should be noted that the bilayers of the micelles of the S3 and G3 sets are thicker than that for the pure PMAcOD evaluated previously:[41] 5.0 nm for the S3 sample and 4.8 nm for the G3 sample compared with 3.2 nm for PMAcOD. This can be explained by partial segregation during micellization. As a result, the total thickness of the bilayers is greater than the double thickness of the completely straightened octadecene tails of PMAcOD, as depicted in Scheme 3. It is also conceivable that the PEG tails contribute to the effective thickness of the models. One should, however, note that the longer PEG chains are too disordered to be captured in the models together with the copolymer heads: our attempts to add longer glycol chains to the MAoCD model did not yield satisfactory fits, neither for the G3 nor for P3 molecules.

3.4. Stability of NPs Coated with Modified PMAOD. In ref 36, encapsulation of magnetic nanoparticles by viral protein cages was reported. Protein cages of brome mosaic virus (BMV) were assembled around negatively charged particles in aqueous buffers. As was shown previously, NPs coated with modified PMAOD acquire a negative charge (Table 3) and display excellent stability in water but immediately salt out in buffer solutions. We expected that grafting of hydrophilic chains to the PMAOD backbone will improve stability of NPs in buffers. The nanoparticles coated with modified PMAOD were dialyzed in a virus capsid reassembly buffer (Tris, 0.05 M; KCl, 0.01 M; $MgCl_2$, 5 mM; pH, 7.39). The P1, P2, G1, and G3 samples aggregated within 20 min, whereas the P3 and P4 samples remained fully soluble even after 24 h. These samples were further dialyzed against 1 M TKM buffer (Tris, 0.01 M; KCl, 1 M; $MgCl_2$, 0.005 M; pH, 7.42), which is used to maintain BMV coat proteins disassembled as dimers. The nanoparticles remained stable for months in that buffer.

4. Conclusions

We established that coating of NPs with modified PMAcOD depends on the length of the grafted tails, which, in turn, determines the types of copolymer micelles in solution as revealed by SAXS. When the 5000 Da PEG or short EG tails are attached to the PMAcOD backbone, the micelles formed (despite the difference of their shapes and ordering) exhibit intermicellar interactions in solution; the latter most likely is the crucial factor for interacting with the OA shell on the NP surface. In contrast, the copolymer formed by the attachment of the 750 Da PEG tails to the PMAcOD backbone forms small, noninteracting micelles that are presumably self-sufficient and do not exhibit interactions with a hydrophobic NP shell, thus preventing NP coating. The importance of this work is in understanding of the connection between the micelle properties and the coating ability when amphiphilic copolymers or other amphiphilic molecules are concerned, which may become a guide for future work on the NP encapsulation.

We synthesized a series of hydrophilic, negatively charged NPs using modified PMAcOD of the P and G series. The TGA data revealed that, for the G and PMAcOD coatings, approximately 400 molecules need to be attached to a single NP to allow its stability in water; the P3 and P4 coatings are successful with only approximately 20 macromolecules, emphasizing the importance of the PEG tails in NP hydrophilization. Among the P-coated samples, only the P3 modified NPs demonstrated both a sufficient negative charge[36] and a good stability in buffers, allowing further studies of virus-like particle formation with these modified cores.

Acknowledgment. This work has been supported, in part, by the NATO Science for Peace Program (Grant No. SfP-981438), NSF award 0631982, NIH award GM081029-01, NSF award 0220560, the IU FRSP grant, and the European Union FP6 Infrastructures Program (Design Study SAXIER, RIDS 011934). B.D. acknowledges partial support from the Indiana METACyt Initiative of Indiana University, funded, in part, through a major grant from the Lilly Endowment, Inc. The measurements at the EMBL beamline X33 at DESY were made within the projects SAXS-06-29 and SAXS-07-29. E.S. and L.B. thank the Federal Program "Scientists and Educators of Innovative Russia" 2009-20013, contract no. 14.740.11.0380. We also thank the IU Nanoscale Characterization Facility for access to the instrumentation.

Supporting Information Available: TEM image of iron oxide nanoparticles, synthesis conditions of modified PMAcOD samples, NMR studies of the degree of grafting, and TGA data. This material is available free of charge via the Internet at http://pubs.acs.org.

References and Notes

(1) Chang, S. Y.; Zheng, N.-Y.; Chen, C.-S.; Chen, C.-D.; Chen, Y.-Y.; Wang, C. R. C. *J. Am. Soc. Mass Spectrom.* **2007**, *18*, 910–918.

(2) Bruls, D. M.; Evers, T. H.; Kahlman, J. A. H.; van Lankvelt, P. J. W.; Ovsyanko, M.; Pelssers, E. G. M.; Schleipen, J. J. H. B.; de Theije, F. K.; Verschuren, C. A.; van der Wijk, T.; van Zon, J. B. A.; Dittmer, W. U.; Immink, A. H. J.; Nieuwenhuis, J. H.; Prins, M. W. J. *Lab Chip* **2009**, *9*, 3504–3510.

(3) Bulte, J. W.; Kraitchman, D. L. *NMR Biomed.* **2004**, *17*, 484–499.

(4) Mulder, W. J. M.; Strijkers, G. J.; van Tilborg, G. A. F.; Griffioen, A. W.; Nicolay, K. *NMR Biomed.* **2006**, *19*, 142–164.

(5) Medarova, Z.; Pham, W.; Farrar, C.; Petkova, V.; Moore, A. *Nat. Med.* **2006**, *13*, 372–377.

(6) Kumagai, M.; Imai, Y.; Nakamura, T.; Yamasaki, Y.; Sekino, M.; Ueno, S.; Hanaoka, K.; Kikuchi, K.; Nagano, T.; Kaneko, E.; Shimokado, K.; Kataoka, K. *Colloids Surf., B* **2007**, *56*, 174–181.

(7) Jain, T. K.; Foy, S. P.; Erokwu, B.; Dimitrijevic, S.; Flask, C. A.; Labhasetwar, V. *Biomaterials* **2009**, *30*, 6748–6756.

(8) Chemla, Y. R.; Crossman, H. L.; Poon, Y.; McDermott, R.; R;, S.; Alper, M. D.; Clarke, J. *Proc. Nat. Acad. Sci.* **2000**, *97*, 14268–14272.

(9) Ivkov, R.; DeNardo, S. J.; Miers, L. A.; Natarajan, A.; Foreman, A. R.; Gruettner, C.; Adamson, G. N.; DeNardo, G. L. *NSTI Nanotech 2006*; Nano Science and Technology Institute: Boston, MA, 2006; Vol. 2, pp 21−24.

(10) Chen, Z. P.; Zhang, Y.; Xu, K.; Xu, R. Z.; Liu, J. W.; Gu, N. *J. Nanosci. Nanotechnol.* **2008**, *8*, 6260–6265.

(11) Das, M.; Mishra, D.; Maiti, T. K.; Basak, A.; Pramanik, P. *Nanotechnology* **2008**, *19*, 415101.

(12) Lu, A.-H.; Salabas, E. L.; Schueth, F. *Angew. Chem., Int. Ed.* **2007**, *46*, 1222–1244.

(13) Talapin, D. V.; Shevchenko, E. V.; Weller, H. In *Nanoparticles*; Schmid, G., Ed.; Wiley-VCH: Weinheim, Germany, 2004; pp 199−230.

(14) Park, T.-J.; Papaefthymiou, G. C.; Viescas, A. J.; Moodenbaugh, A. R.; Wong, S. S. *Nano Lett.* **2007**, *7*, 766–772.

(15) Rong, C.-B.; Li, D.; Nandwana, V.; Poudyal, N.; Ding, Y.; Wang, Z. L.; Zeng, H.; Liu, J. P. *Adv. Mater.* **2006**, *18*, 2984–2988.

(16) Hellstern, D.; Schulze, K.; Schopf, B.; Petri-Fink, A.; Steitz, B.; Kamau, S.; Hilbe, M.; Koch-Schneidemann, S.; Vaughan, L.; Hottiger, M.; Hofmann, M.; Hofmann, H.; von Rechenberg, B. *J. Nanosci. Nanotechnol.* **2006**, *6*, 3261–3268.

(17) Briley-Saebo, K.; Bjornerud, A.; Grant, D.; Ahlstrom, H.; Berg, T.; Kindberg, G. M. *Cell Tissue Res.* **2004**, *316*, 315–323.

(18) Sun, S.; Zeng, H. *J. Am. Chem. Soc.* **2002**, *124*, 8204–8205.

(19) Li, Z.; Chen, H.; Bao, H.; Gao, M. *Chem. Mater.* **2004**, *16*, 1391–1393.

(20) Redl, F. X.; Black, C. T.; Papaefthymiou, G. C.; Sandstrom, R. L.; Yin, M.; Zeng, H.; Murray, C. B.; O'Brien, S. P. *J. Am. Chem. Soc.* **2004**, *126*, 14583–14599.

(21) Yu, W. W.; Falkner, J. C.; Yavuz, C. T.; Colvin, V. L. *Chem. Commun.* **2004**, 2306–2307.

(22) Park, J.; An, K.; Hwang, Y.; Park, J.-G.; Noh, H.-J.; Kim, J.-Y.; Park, J.-H.; Hwang, N.-M.; Hyeon, T. *Nat. Mater.* **2004**, *3*, 891–895.

(23) Kwon, S. G.; Piao, Y.; Park, J.; Angappane, S.; Jo, Y.; Hwang, N.-M.; Park, J.-G.; Hyeon, T. *J. Am. Chem. Soc.* **2007**, *129*, 12571–12584.

(24) Jana, N. R.; Chen, Y.; Peng, X. *Chem. Mater.* **2004**, *16*, 3931–3935.

(25) Jun, Y.-W.; Huh, Y.-M.; Choi, J.-S.; Lee, J.-H.; Song, H.-T.; Kim, S.; Yoon, S.; Kim, K.-S.; Shin, J.-S.; Suh, J.-S.; Cheon, J. *J. Am. Chem. Soc.* **2005**, *127*, 5732–5733.

(26) Gussin, H. A.; Tomlinson, I. D.; Little, D. M.; Warnement, M. R.; Qian, H.; Rosenthal, S. J.; Pepperberg, D. R. *J. Am. Chem. Soc.* **2006**, *128*, 15701–15713.

(27) Zhang, Q.; Gupta, S.; Emrick, T.; Russell, T. P. *J. Am. Chem. Soc.* **2006**, *128*, 3898–3899.

(28) Han, G.; Ghosh, P.; Rotello, V. M. *Nanomedicine* **2007**, *2*, 113–123.

(29) Hostetler, M. J.; Templeton, A. C.; Murray, R. W. *Langmuir* **1999**, *15*, 3782–3789.

(30) Wan, S.; Huang, J.; Guo, M.; Zhang, H.; Cao, Y.; Yan, H.; Liu, K. *J. Biomed. Mater. Res.* **2007**, *80A*, 946–954.

(31) Kang, Y.; Taton, T. A. *Macromolecules* **2005**, *38*, 6115–6121.

(32) Korth, B. D.; Keng, P.; Shim, I.; Bowles, S. E.; Tang, C.; Kowalewski, T.; Nebesny, K. W.; Pyun, J. *J. Am. Chem. Soc.* **2006**, *128*, 6562–6563.

(33) Nitin, N.; LaConte, L. E. W.; Zurkiya, O.; Hu, X.; Bao, G. *JBIC, J. Biol. Inorg. Chem.* **2004**, *9*, 706–712.

(34) Dubertret, B.; Skourides, P.; Norris, D. J.; Noireaux, V.; Brivanlou, A. H.; Libchaber, A. *Science* **2002**, *298*, 1759–1762.

(35) Lim, Y. T.; Lee, K. Y.; Lee, K.; Chung, B. H. *Biochem. Biophys. Res. Commun.* **2006**, *344*, 926–930.

(36) Huang, X.; Bronstein, L. M.; Retrum, J. R.; Dufort, C.; Tsvetkova, I.; Aniagyei, S.; Stein, B.; Stucky, G.; McKenna, B.; Remmes, N.; Baxter, B.; Kao, C. C.; Dragnea, B. *Nano Lett.* **2007**, *7*, 2407–2416.

(37) Shtykova, E. V.; Huang, X.; Remmes, N.; Baxter, D.; Stein, B. D.; Dragnea, B.; Svergun, D. I.; Bronstein, L. M. *J. Phys. Chem. C* **2007**, *111*, 18078–18086.

(38) Pellegrino, T.; Manna, L.; Kudera, S.; Liedl, T.; Koktysh, D.; Rogach, A. L.; Keller, S.; Raedler, J.; Natile, G.; Parak, W. J. *Nano Lett.* **2004**, *4*, 703–707.

(39) Yu, W. W.; Chang, E.; Sayes, C. M.; Drezek, R.; Colvin, V. L. *Nanotechnology* **2006**, *17*, 4483–4487.

(40) Di Corato, R.; Quarta, A.; Piacenza, P.; Ragusa, A.; Figuerola, A.; Buonsanti, R.; Cingolani, R.; Manna, L.; Pellegrino, T. *J. Mater. Chem.* **2008**, *18*, 1991–1996.

(41) Shtykova, E. V.; Gao, X.; Huang, X.; Dyke, J. C.; Schmucker, A. L.; Remmes, N.; Baxter, D. V.; Stein, B.; Dragnea, B.; Konarev, P. V.; Svergun, D. I.; Bronstein, L. M. *J. Phys. Chem. C* **2008**, *112*, 16809–16817.

(42) Yu, W. W.; Chang, E.; Falkner, J. C.; Zhang, J.; Al-Somali, A. M.; Sayes, C. M.; Johns, J.; Drezek, R.; Colvin, V. L. *J. Am. Chem. Soc.* **2007**, *129*, 2871–2879.

(43) Bronstein, L. M.; Huang, X.; Retrum, J.; Schmucker, A.; Pink, M.; Stein, B. D.; Dragnea, B. *Chem. Mater.* **2007**, *19*, 3624–3632.

(44) Roessle, M. W.; Klaering, R.; Ristau, U.; Robrahn, B.; Jahn, D.; Gehrmann, T.; Konarev, P.; Round, A.; Fiedler, S.; Hermes, C.; Svergun, D. *J. Appl. Crystallogr.* **2007**, *40*, s190–s194.

(45) Konarev, P. V.; Volkov, V. V.; Sokolova, A. V.; Koch, M. H. J.; Svergun, D. I. *J. Appl. Crystallogr.* **2003**, *36*, 1277–1282.

(46) Svergun, D. I. *J. Appl. Crystallogr.* **1992**, *25*, 495–503.

(47) Svergun, D. I. *Biophys. J.* **1999**, *76*, 2879–2886.

(48) Svergun, D. I.; Barberato, C.; Koch, M. H. J. *J. Appl. Crystallogr.* **1995**, *28*, 768.

JP107283W